Materials Research. 2013; 16(1): 204-214
DOI: 10.1590/S1516-14392012005000171
© 2013

Influence of the Microstructure on the Electrochemical Properties of Al-Cr-N Coatings Deposited by Co-sputtering Method from a Cr-Al Binary Target

Oscar Mauricio Sánchez Quintero[a]*, *Willian Aperador Chaparro*[b], *Leonid Ipaz*[a],

Jaime Eduardo Sánchez Barco[a], *Francisco Espinoza Beltrán*[c], *Gustavo Zambrano*[a]

[a]*Thin Films Group, Universidad del Valle, Calle 13 no. 100-00, A.A. 25360, Cali, Colombia*
[b]*Department of Mechatronic Engineering, Universidad Militar Nueva Granada, Carrera 11 no. 101-80, Bogotá, Colombia*
[c]*Center for Research and Advanced Studies – CINVESTAV-IPN, Querétaro, México*

Received: June 27, 2012; Revised: September 4, 2012

In the present paper, aluminum chromium nitride (Al-Cr-N) films were deposited onto AISI H13 steel substrates by a reactive d.c magnetron co-sputtering system in an atmosphere of Ar/N_2 (90/10) gas mixture from a binary target composed of chromium (99.95%) and aluminum (99.99%). Different powers (40, 50, 60, and 70 W) were applied to the target, in order to study the effect of this parameter and the sputtering yield of binary target, on the microstructure and the electrochemical properties of the Al-Cr-N coatings. The corrosion behavior in 3.5 wt. (%) NaCl solution was investigated by electrochemical corrosion tests (Tafel polarization curves and Electrochemical Impedance Spectroscopy (EIS)), and the chemical composition, microstructure and the absorption bands by means of Energy Dispersive X-ray Spectroscopy (EDX), X-ray diffractometry (XRD) and Fourier Transform Infrared Spectroscopy (FTIR), respectively. EIS results showed that the Al-Cr-N coating deposited at 40 W, exhibited the lower porosity and the highest polarization resistance, and subsequently, when the power applied to the binary target increased, the corrosion rate and the porosity increase.

Keywords: *thin films, electrochemical properties, co-sputtering, aluminum chromium nitride*

1. Introduction

In many industrial applications, metal nitride hard coatings are commonly used[1-5]. Currently, the properties required by these coatings are not only focused on durability or hardness, as on the extreme conditions of production. For this reason, the work tools require combining those properties with corrosion resistance. Such coatings are usually deposited by PVD techniques, allowing the formation of thick films, as well as high adherence to the substrate. Additionally, deposition needs to be performed at low temperatures[6,7] to avoid microstructural changes that will occur in the steel substrate. Chromium nitride has been successfully applied in molding dies, wear components, cutting tools, including metal processing devices, because of its superior corrosion resistance and relatively high hardness and wear resistance[8-11]. Recently, Al-Cr-N ternary coatings have also shown better resistance to oxidation[12-16], given that chromium and aluminum can form protective oxides that suppress oxygen diffusion. The aim of this work is to study the effect of varying the applied power to the binary Cr-Al target in a (Ar/N_2) gas mixture on the structural and electrochemical properties of Cr-Al-N films deposited by the dc reactive magnetron co-sputtering technique. The chemical composition was determined by Energy Dispersive X-ray spectroscopy (EDX), the crystallographic structure by X-ray diffractometry (XRD), chemical bonds in the films were examined by Fourier Transform Infrared (FTIR) spectroscopy, and electrochemical properties were characterized via Electrochemical Impedance Spectroscopy (EIS) and Tafel polarization curves. Finally, the degradation process of the films was qualitatively analyzed by optical microscopy.

*e-mail: oscar.sanchez@correounivalle.edu.co

2. Experimental Details

Aluminum chromium nitride (Al-Cr-N) films were deposited onto AISI H13 steel substrates by reactive d.c. magnetron co-sputtering system in an Ar/N_2 (90/10) gas mixture from a metallic binary target (1:1 area ratio Cr-Al) composed of chromium (99.95%) and aluminum (99.90%), by applying different powers to the target (40, 50, 60, and 70 W) to study the effect of this parameter on the microstructural and electrochemical properties of the Al-Cr-N coatings. The chemical composition of the hot working tool steel (AISI H13) is listed in Table 1. Samples were mechanically polished using 1200 grit SiC for the final step. After this, samples were polished with 0.5 μm alumina slurry. The substrates were then cleaned ultrasonically in acetone for 10 minutes. The deposition chamber was evacuated to a base pressure of 5.0×10^{-4} mbar, and the

Table 1. Chemical composition of AISI H13 steel in wt. (%).

Element	C	Si	Mn	S	Cr	Mo	V
Content (wt. %)	0.40	0.99	0.37	0.01	5.12	1.25	0.90

working pressure was 2.8×10^{-3} mbar. The binary target and substrate were sputter-cleaned for 20 minutes, before film growth. A buffer layer of Al-Cr with a thickness about 100 nm, was previously deposited for 4 minutes in order to improve the adhesion Al-Cr-N to the steel substrate. During the deposition process of Al-Cr-N coating for 1 hour, the substrate temperature (400 °C), and the target-substrate distance (5.0 cm) were kept constant.

Superficial characteristics were determined using Scanning Electron Microscopy (SEM) equipped with a high sensibility detector (multi-mode) for scattering electrons. The chemical composition of the single layer coatings was determined by energy dispersive x-ray (EDX) analysis with a high-purity Ge EDX detector for the reliable acquisition of EDX spectra using a Philips XL 30 FEG. Analyses to identify the characteristic bonds at single layer systems were done by Fourier Transformed Infrared spectroscopy (FTIR) in transmittance mode using a Shimatzu 8000 (600-3500 cm^{-1}) spectrometer which uses a Nerst ceramic source.

The thicknesses of Al-Cr-N single-layered system were obtained by means of a Dektak 3030 profilometer.

The electrochemical study was carried out with a Gamry PCI4300™ Potentiostat, which has a Gamry Framework Version 4.21/EIS 300 software, through Electrochemical Impedance Spectroscopy (EIS) and Tafel polarization curves techniques at room temperature by using a cell (300 mL volume) with a conventional three-electrode configuration, which uses a working electrode of an Al-Cr-N sample within an exposed area of 1 cm^2, a reference electrode (Ag/AgCl), and a platinum wire counter-electrode under 3.5% NaCl solution with distilled water. The electrochemical behavior of the electrolyte was studied by using Electrochemical Impedance Spectroscopy (EIS) at the Open Circuit Potential for 30 minutes to establish stable Open Circuit Potential (OPC) values at which the EIS measurements were initiated. For Nyquist diagrams, frequency sweeps were conducted in the range of 10^4 to 10^{-3} Hz, using a sinusoidal voltage perturbation with signal amplitude of 10 mV. Measurements were carried out on a set of three different replicate samples. Anodic polarization curves were recorded at room temperature (~25 °C) after 30 minutes exposure to the test solution, in a 3.5% NaCl aqueous solution (pH ~ 8). All potentiodynamic measurements were performed at a potential scanning rate of 0.16 mV/s. The potential range was from −250 mV to 250 mV vs. OCP. The degradation of Al-Cr-N films, depending on the attack in the NaCl aqueous solution, was monitored by an optical Olympus PME-3 microscope.

3. Results and Discussion

3.1. *EDX and SEM analysis*

The morphology of the films deposited at different sputtering powers is shown in Figure 1. As can see from these micrographs, our Al-Cr-N coatings does not present

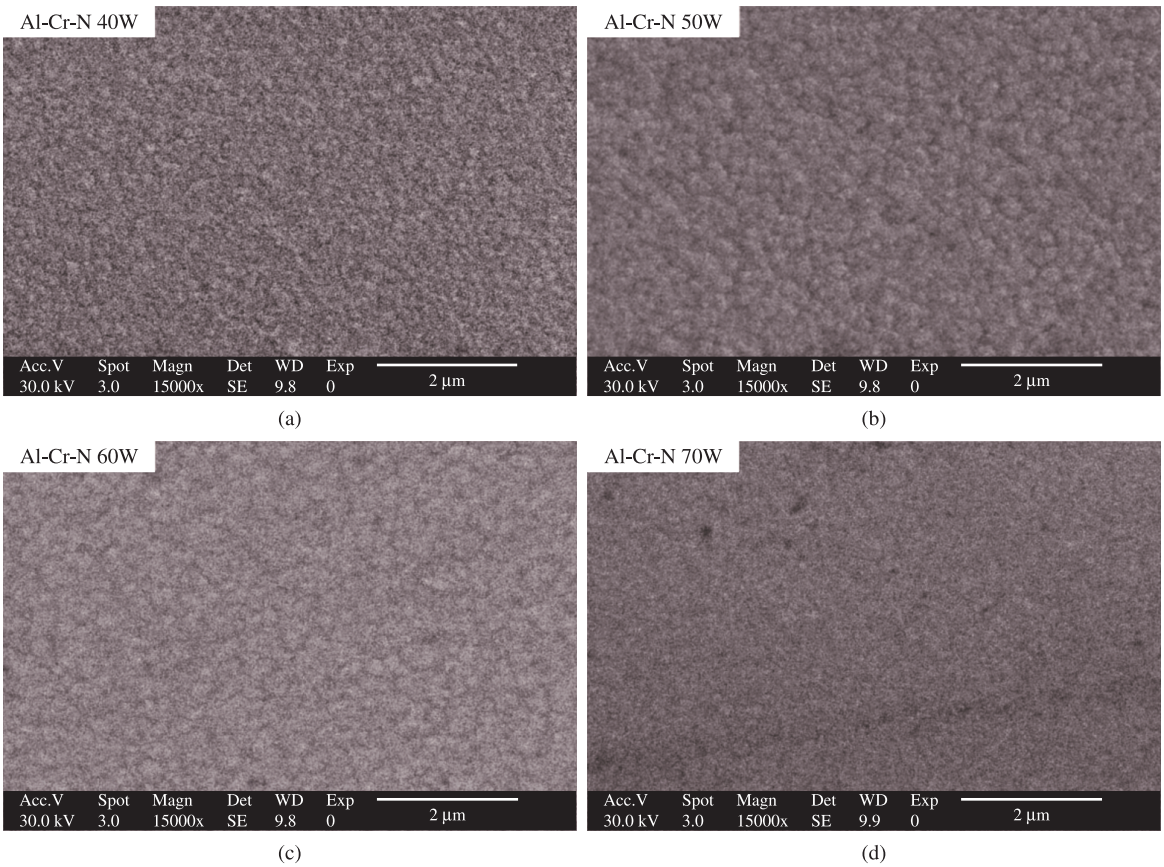

Figure 1. SEM micrographs of Cr-Al-N coatings at different applied powers.

big shallow craters, cone structures or dish-like holes arising from wrenching of the cone structure, but as can be seen from the SEM images, they present pin-holes that could extending through the whole coating, which are originated from a small hole in the substrate due to its mechanical polished, until the PVD process[17]. EDX analysis of the deposited Al-Cr-N coatings is shown in Figure 2. The different power applied to the binary target has an obvious effect over atomic concentrations. While the N keeps practically constant, the oxygen presents the higher concentration (~25%) at 40 and 50 W and decreases to the approximately 17% at 60 and 70 W. On the other hand, when the power applied to the binary target is increased, the Cr concentration has a tendency to reach a saturation value, while the Al after 50 W power, shows a tendency to keep constant.

3.2. *XRD analysis*

The XRD patterns for the Al-Cr-N coatings, deposited at powers of 40, 50, 60, and 70 W, are shown in Figure 3. It can be seen that for an applied power of 40 W, the main peak in the XRD pattern corresponds to the coexistence of the reflection planes (111) at $2\theta = 37°$ and (101) at $2\theta = 38°$[18], associated to the cubic (c) and hexagonal (h) phases of CrN and AlN, respectively. When the power applied to the target increases, a peak emerges at $2\theta = 31.7°$, corresponding to the (220) reflection plane of AlN cubic phase, which disappears at 60 W. Additionally, from XRD patterns at 60 and 70 W the evolution of the (100) reflection planes can be observed at $2\theta = 33.2°$, corresponding to the h-AlN phase. In contrast, the peaks that emerge at $2\theta = 38.5°$ and $2\theta = 44.7°$, are associated to the (111) and (200) reflection planes of Al-Cr cubic phase, respectively. This phase behavior can be attributed to increase of the applied power in a binary target of Al-Cr (1:1), which can promote the formation of Al-Cr phase instead of the Al-Cr-N phase. Particularly, at 70 W the (100) reflection plane of h-AlN phase increases, whereas the (111) and (200) reflection plane decreases, showing the phase change from B1 to B4 type. This is because at low Ar^+ ion energies, the Cr sputtering yield (Y_{Cr}) is higher than the Al sputtering yield (Y_{Al}), approximately $Y_{Cr}/Y_{Al} = 2$ or 3[19], then at a power of 40 W, the lowest power, the atomic percent of Cr in the coatings is higher that aluminum, which it is possible that favors the CrN cubic phase with a few substitutions of Cr atoms by Al atoms in the crystalline structure. The XRD result for 40 W confirmed the coexistence of CrN and AlN phases. With the increase of the power applied to the Cr-Al binary target, also increase the amount of Cr deposited on the coating until a saturation value, while the amount of aluminum, after 50 W power, shows a tendency to keep approximately constant, causing the emerge of Al-N phases. However, with the increase of the applied power, the ion energy of Ar^+ increases as well, and for this reason, the Al sputtering yield is approximately similar to the Cr sputtering yield[19], inducing probably the formation of more amount of c-Al-Cr phase than Al-N phase. Additionally, it can observed in the patterns an irregular changes of the (200) plane reflection at $2\theta = 44.20°$, related to the CrN cubic phase. Likewise, in the film deposited at a power of 70 W (211) plane reflection presented at $2\theta = 61.73°$, related to the hexagonal phase of CrN[18,20,21].

3.3. *FTIR analysis*

Figure 4 shows FTIR spectra of the Al-Cr-N coatings identifying the vibration bands corresponding to the energy absorption of the active modes around 500 cm^{-1} related to the Cr-N bonds, as well as the vibration bands at 640 cm^{-1}, 780 cm^{-1}, 1025 cm^{-1}, associated to the Al-N bonds. Additionally, at 470, 600, and 650 cm^{-1}, the Cr-O and Al-O oxide bands appear, which is characteristic of these coatings[22-24]. In conclusion, as can be seen from the FTIR spectra they indirectly confirm the results obtained by XRD because the absorption bands associated to the

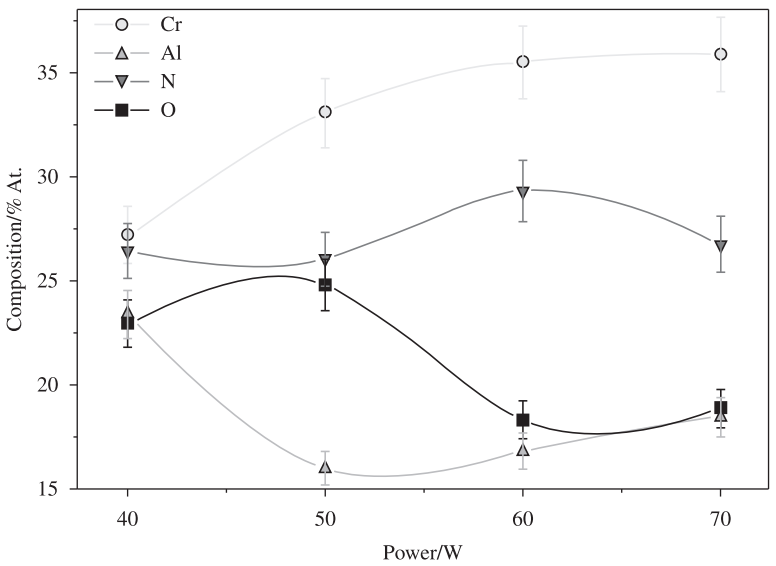

Figure 2. Atomic percentage of Al-Cr-N coatings as function of the different applied powers.

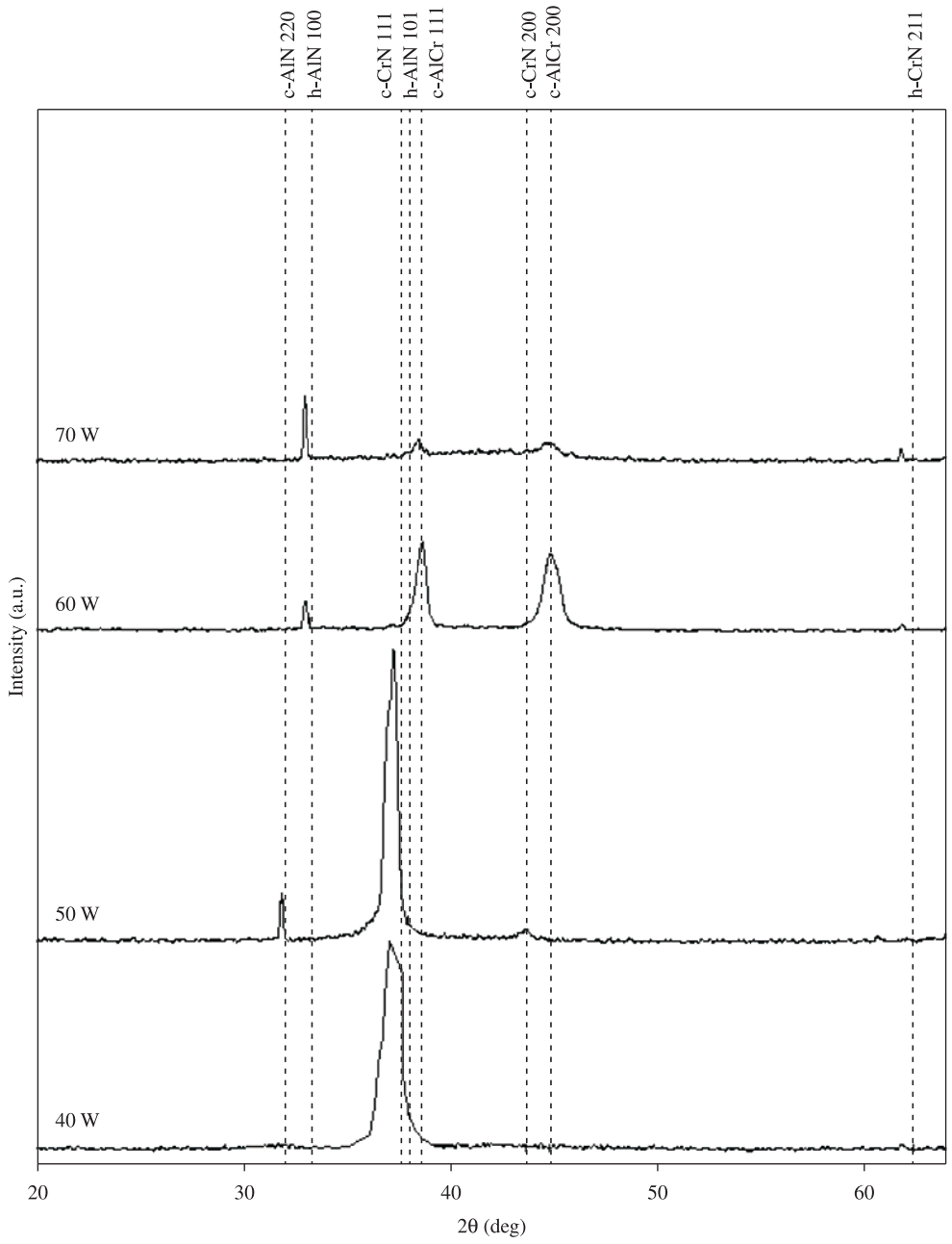

Figure 3. XRD patterns for the Al-Cr-N coatings obtained at different applied powers.

active vibration modes of Al-N and Al-Cr-N phases have higher transmittance percentage (~5%) at 40 W power than for greater powers.

3.4. *EIS analysis*

Figure 5 shows the Nyquist plots of the substrate and Al-Cr-N coatings immersed in a solution of 3.5% NaCl. In all Nyquist plots shows a capacitive behavior at high frequencies, which defines a flat semi-circle whose center is located below the real axis (the center of the Nyquist plot is rotated below the real axis with an angle Φ).This phenomenon of flattening of the semicircle is associated with a process of dispersion in the frequency, because the electrode surface is not homogeneous. Additionally, there is a diffusion process that aims to define a second semicircle at low frequencies. A capacitive depressed semicircle at high frequencies (HF) and a pseudo-inductive semicircle appearing in the fourth quadrant at low frequencies (LF) can be observed. Figure 5 also includes the simulated data, performed by using the equivalent

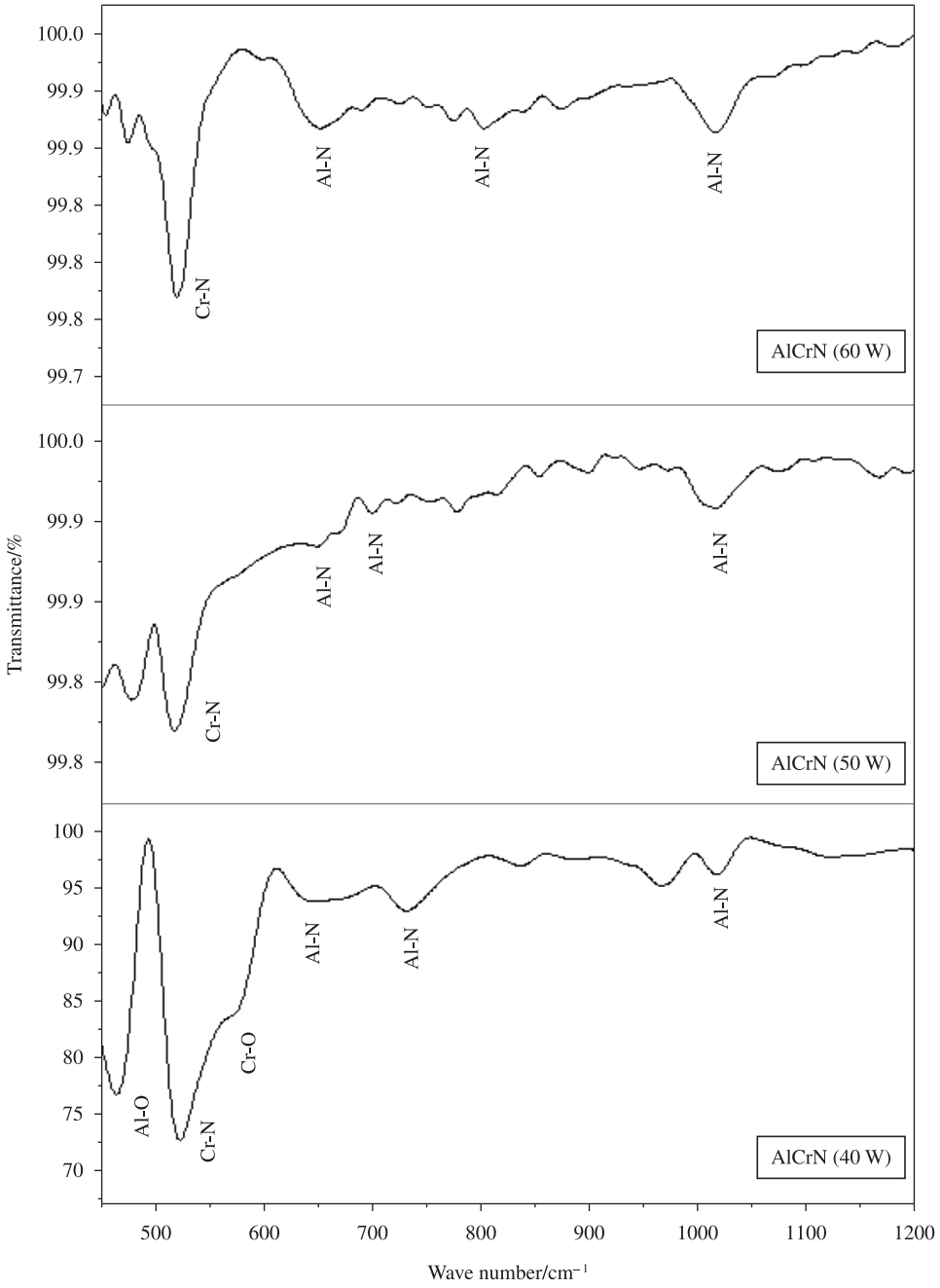

Figure 4. FTIR spectra of Al-Cr-N coatings deposited at different applied powers.

circuit from Figure 6. The EIS data were interpreted based on proposed equivalent electrical circuits using a suitable fitting procedure elaborated by Gammy Echem Analyst™ software. The results of the analysis and calculations of the impedance data (averaged from three replicate specimens) are given in Figure 5. An excellent agreement between the experimental and simulated data is confirmed. Table 2 shows the values of the parameters used in the simulation. A constant phase element [CPE_1: $Y = Y_p(j\omega)^{\alpha}$] in parallel with the charge transfer resistance (R_{ct}) is modelling the HF semicircle, which represent the behaviour of electrolyte/coating interface, and could be influenced by roughness, pores, or grow defects. The R_{ct} parameter is in series with a combination of a second constant phase element [CPE_2: $Y = Y_q(j\omega)^{\beta}$] in parallel with the adsorption resistance (R_{ad}), representing a pseudo-adsorption process semicircle defined at LF and appearing in the fourth quadrant, and it is related with the electrolyte/steel interface (via defects) connected to the charge transfer resistance in the double layer capacitance[9,10,25-27]. Here Y_p and Y_q are the frequency

independent constants, $j^2 = (-1)$, ω is the angular frequency, and the exponents α and β are between $0 < \alpha, \beta < 1$. Finally, the R_s parameter is the electrolyte resistance. The values of α and β (Table 2), corresponds to the exponential coefficient of the phase angle shift ($\pi/2$). The values of α for the coatings and the substrate at high frequency CPE_1 are in the range

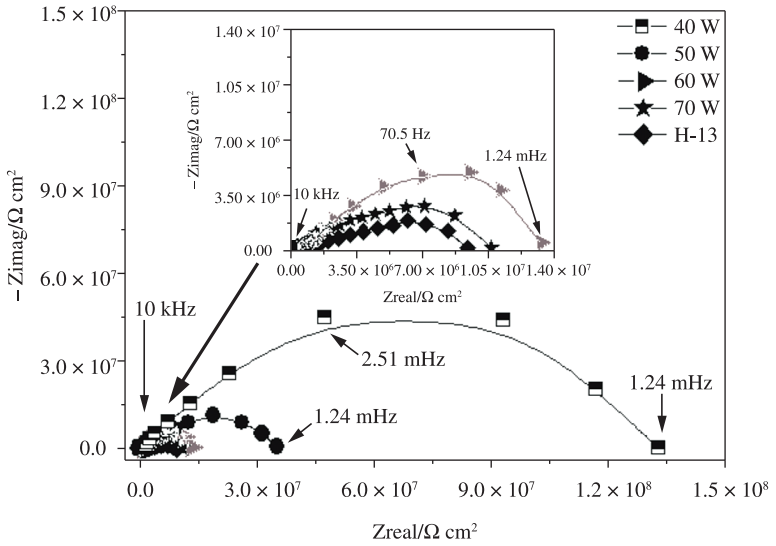

Figure 5. EIS curves for uncoated AISI H13 steel substrate and coated with Al-Cr-N films, deposited at different powers.

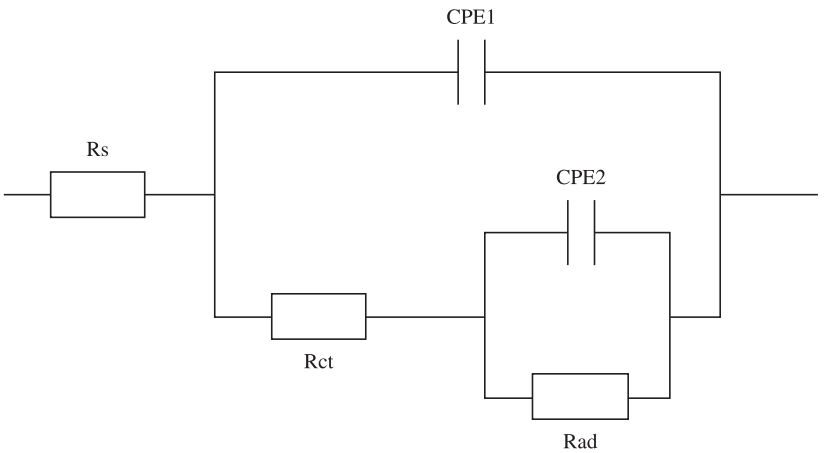

Figure 6. Electrical equivalent circuit for the Randles cell.

Table 2. Parameters obtained from the fitting procedure of impedance data for EIS curves for uncoated AISI H13 steel substrate and coated with Al-Cr-N films, deposited at different powers and immersed in a 3.5% NaCl solution.

	R_s $\Omega\ cm^2$	CPE_1 $\mu F\ cm^{-2}\ s^{-(1-\beta)}$	α	R_{ct} $10^6\ \Omega\ cm^2$	CPE_2 $\mu F\ cm^{-2}\ s^{-(1-\beta)}$	β	R_{ad} $10^6\ \Omega\ cm^2$
40 W	32.12 (0.3%)	76.21 (2.3%)	0.83 (0.4%)	29.45 (3.2%)	4.68 (2.8%)	0.91 (0.5%)	95.32 (6%)
50 W	41.5 (0.5%)	42.41 (2.4%)	0.86 (0.5%)	11.21 (4.2%)	1.59 (1.8%)	0.64 (0.3%)	36.41 (5%)
60 W	34.8 (0.4%)	68.5 (1.3%)	0.82 (0.2%)	3.64 (4.2%)	1.31 (2.3%)	0.78 (0.4%)	10.05 (4%)
70 W	42.5 (0.5%)	54.36 (3.3%)	--	1.21 (4%)	0.88 (2.5%)	0.70 (0.3%)	8.42 (3%)
Substrate	32.1 (0.5%)	21.5 (3.4%)	0.58 (0.5%)	9.07 (5%)			

of 0.58 to 0.86, indicating that the roughness of the surface generates a charge distribution. To low frequency CPE_2 shows a β of 0.64 for 50 W and 0.70 for 70 W, indicating the presence of migration or diffusion of species, and at 40 and 60 W the β values are 0.91 and 0.78, respectively, generating density distribution of charge carriers, i.e., a double layer with a complex structure.

The coating obtained at a power of 40 W shows better polarization resistance values than the coatings deposited at higher powers. The film deposited at a power of 70 W displays the lowest polarization resistance value; however, it shows a higher value than the uncoated AISI H13 steel.

Figure 7 shows typical polarisation curves for AISI H13 steel after 30 minutes of immersion in a 3.5% NaCl aqueous test solution at room temperature, and with a scan rate of 0.16 mV/s^{-1}. A similar shape is observed in the four polarisation curves of Al-Cr-N deposited coatings. The anodic polarization curves shown in Figure 7 indicate that the H13 steel in 3.5% NaCl has a change in their behavior on the anodic branch after the region between potential corrosion, near to the potential of –0.87 $V_{Ag/AgCl,}$ and a potential value of –0.80 $V_{Ag/AgCl}$. This change can be defined as the beginning of the formation of a weak and thin layer of passivation, whose stability is poor, because after the potential reaches a value of –0.80 $V_{Ag/AgCl}$, it shows a gradual increase in current density, and then an increase in the dissolution rate of the steel substrate. This suggests that the kinetics of the process is dominated by diffusion, showing a metal dissolution in the evaluated anodic region[28]. Al-Cr-N coatings deposited with 40 W, 50 W, 60 W and 70 W, have general corrosion, but the increase in current density is low. Arriving at a potential close to 0.40 $V_{Ag/AgCl}$ and –0.10 $V_{Ag/AgCl}$ for 50 W and 70 W respectively increases the decomposition reaction indicating an increase in corrosion rate. Therefore, the Tafel polarization curves show that Al-Cr-N coating samples deposited on the AISI H13 steel substrate at a power of 40 W are less reactive or more resistant to corrosion than AISI H13/Al-Cr-N systems deposited at higher powers, being the AISI H13/Al-Cr-N system deposited at 70 W power the most active. The last results agree with the EIS results, and it present in Table 3.

As it is known, corrosion behavior is not only due to the intrinsic properties of the coating, but also a result of small structural defects, such as pores and micro-cracks, formed during deposition. With the development of electrochemical techniques, it is possible to obtain, besides the corrosion behavior, the porosity (P) of the coatings. Under the assumption that coating is nobler than steel substrate, implies that the corrosion rate of the coating is much less compared with the steel corrosion rate that is obviously the case for the

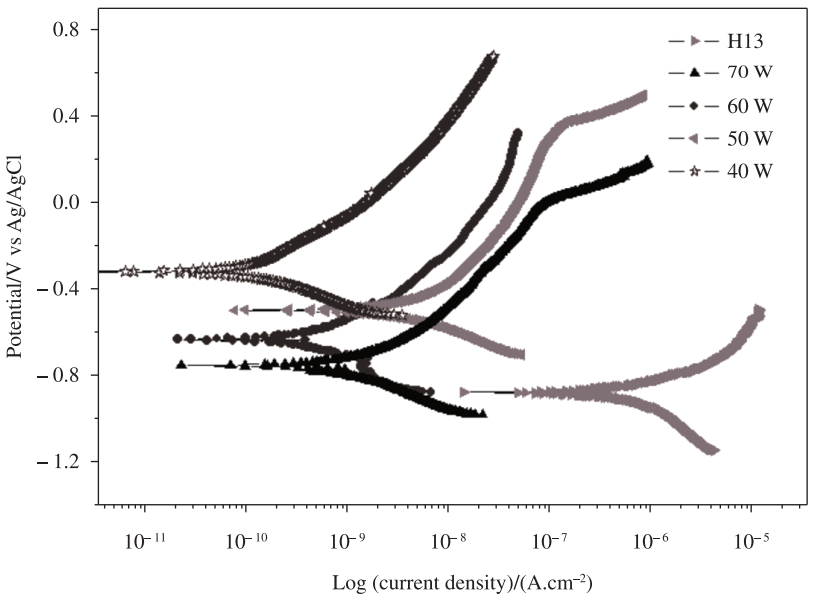

Figure 7. Tafel polarization curves for uncoated AISI H13 steel substrate and coated with Al-Cr-N films, deposited at different powers.

Table 3. Potentiodynamic test results.

Specimen	E_{corr} (mV)	β_a (mV/decade)	β_c (mV/decade)	R_p (Ω-cm²)
H13 Steel	–886	444.9	4.6	9.04×10^6
H13/AlCrN 40 W	–321	310.2	191.9	1.33×10^8
H13/AlCrN 50 W	–501	552.5	272.4	3.51×10^7
H13/AlCrN 60 W	–637	185.6	126.1	1.23×10^7
H13/AlCrN 70 W	–760	329.5	283.9	8.67×10^6

steel protected by nitride coatings, we can use the empirical equation established by B. Mathes et al.[29,30] to determinate the porosity of the coatings:

$$P(\%) = \left[\frac{R_{p,s}}{R_{p,f}} \times 10^{-\left[\Delta E_{corr}/\beta_\alpha\right]} \right] \times 100 \quad (1)$$

where $R_{p,s}$ is the polarization resistance of the substrate, $R_{p,f}$ the polarization resistance of coating-substrate system, ΔE_{corr} the corrosion potential difference between the substrate and coating layer, and β_a the anodic Tafel constant of substrate. These values of i_{coor}, corrosion rate and porosity were calculated by Equations 1-3, respectively, and are presented in Table 4.

From Table 4 we can observe how the porosity increase and polarization resistance decreases when the power applied to the binary target, increase. The porosity formed during the deposition process is because when we increasing the power applied to the Al-Cr binary target, the Al and Cr atoms becomes more energetic, producing a re-sputtering phenomenon on the coatings surface, additionally, as was indicated before in the SEM micrograph, we can observe the presence of pin-holes in the coatings, consequently, these two effects produce the increase of the electrolyte diffusion through the open porosity to the substrate[31]. When chloride ions (Cl^-) spread by capillarity penetrate the pores and other defects, the exposed area begins to experiment an anodic dissolution that generally is propagated laterally, increasing the corrosion rate due to the coating represents a cathode area much larger than the anodic pore area[32]. Coatings growths at high powers (60 and 70 W) had a higher localized corrosion attack on the interfaces evidenced by the decrease of the polarization resistance of the substrate-coating interface (see R_{ad} in Table 2).

On the other hand, it can be seen from the Table 4, when the power applied to the Cr-Al binary target increases, the polarization resistance (R_p) decreases which it is an indicative that the corrosion rate increases; however, as expected, the thickness of the Al-Cr-N films, increases (Table 5). This may be related to the microstructure of the coatings, which, for films deposited at a power of 40 W, is dominated by the cubic crystal structure of the Al-Cr-N, and at higher powers, the microstructure is composed of a mixture of the cubic and hexagonal phases of Al-Cr-N, Cr-N, and Al-Cr, with the cubic phase of Al-Cr-N being the most important from the standpoint of corrosion resistance[10]. This phase change in the coatings associated to the variation of the applied power causes a decrease of the corrosion resistance, which can be related to a possible saturation in the amount of Cr and an increase of Al content in the films, when the power applied to the Cr-Al binary target, increases. This effect was confirmed by EDX and XRD results (see Figures 2 and 3). Furthermore, as was showed in Figure 2, the presence of oxygen is higher in the coatings deposited at lower applied powers (40 and 50 W) than at higher powers (60 and 70 W). This implies that in the deposition chamber there is the oxygen presence, owing to the residual water vapor. Taking into account the high oxygen affinity with aluminum and chromium, it is probable the growth of Al and Cr protective oxides at lower powers, which improve the corrosion resistance behavior of the all protective system. FTIR analysis confirms the presence of Cr-O and Al-O bands at those lower applied powers.

Table 4. Polarization resistance (R_p), current density (i_{corr}), and porosity (P) of AISI H13/Al-Cr-N system deposited at different powers compared to the H13 steel.

Specimen	i_{corr} (nA/cm²)	R_p (Ω-cm²)	P (%)
H13 Steel	3.290	9.04×10^6	---
H13/AlCrN 40 W	0.147	1.33×10^8	0.7
H13/AlCrN 50 W	7.010	3.51×10^7	5.3
H13/AlCrN 60 W	0.333	1.23×10^7	35.9
H13/AlCrN 70 W	1.690	8.67×10^6	40.6

Table 5. Al-Cr-N coating thickness dependence of the power applied to the Cr-Al binary target.

Specimen	Thickness (μm)
H13/AlCrN 40 W	1.7
H13/AlCrN 50 W	1.9
H13/AlCrN 60 W	2.1
H13/AlCrN 70 W	2.7

3.5. *Optical microscopy analysis*

To determine the degradation suffered by the AISI H13 steel substrate with and without Al-Cr-N coatings under the effect of the saline (3.5% NaCl) solution, Al-Cr-N coatings were analyzed by using optical microscopy images. Figure 8 shows the result of the attack on the exposed surfaces generated by the migration of Cl^- ions through the coating, showing localized corrosion damage "pits". This effect on the coatings increased when the deposition power applied to the target increased from 40 to 70 W.

The H13/Al-Cr-Al system presenting better properties was obtained at a power of 40 W applied to the target, and it can be observed in Figure 8b that this system does not present significant damage on its surface creating a good corrosion protection for the H13 steel substrate. Contrary to this behavior, coatings deposited at 50, 60, and 70 W present more significant degradation (Figure 8c-e) visually confirm the results obtained by EIS analysis.

4. Conclusions

In the present study, the influence of the power applied to the metallic binary target (1:1 area ratio Cr-Al), on the formation of Al-Cr-N phases obtained by co-sputtering and their subsequent electrochemical behavior has been evidenced. The results showed, however, that by increasing the power applied to the target, the thickness of the Al-Cr-N films also increases, but the coating presenting greater corrosion resistance was deposited at 40 W (thickness of 1.7 microns) a property that decreased as layer thickness increased (up to 2.7 microns). This is related to the evolution of the phases present in each of the coatings deposited at

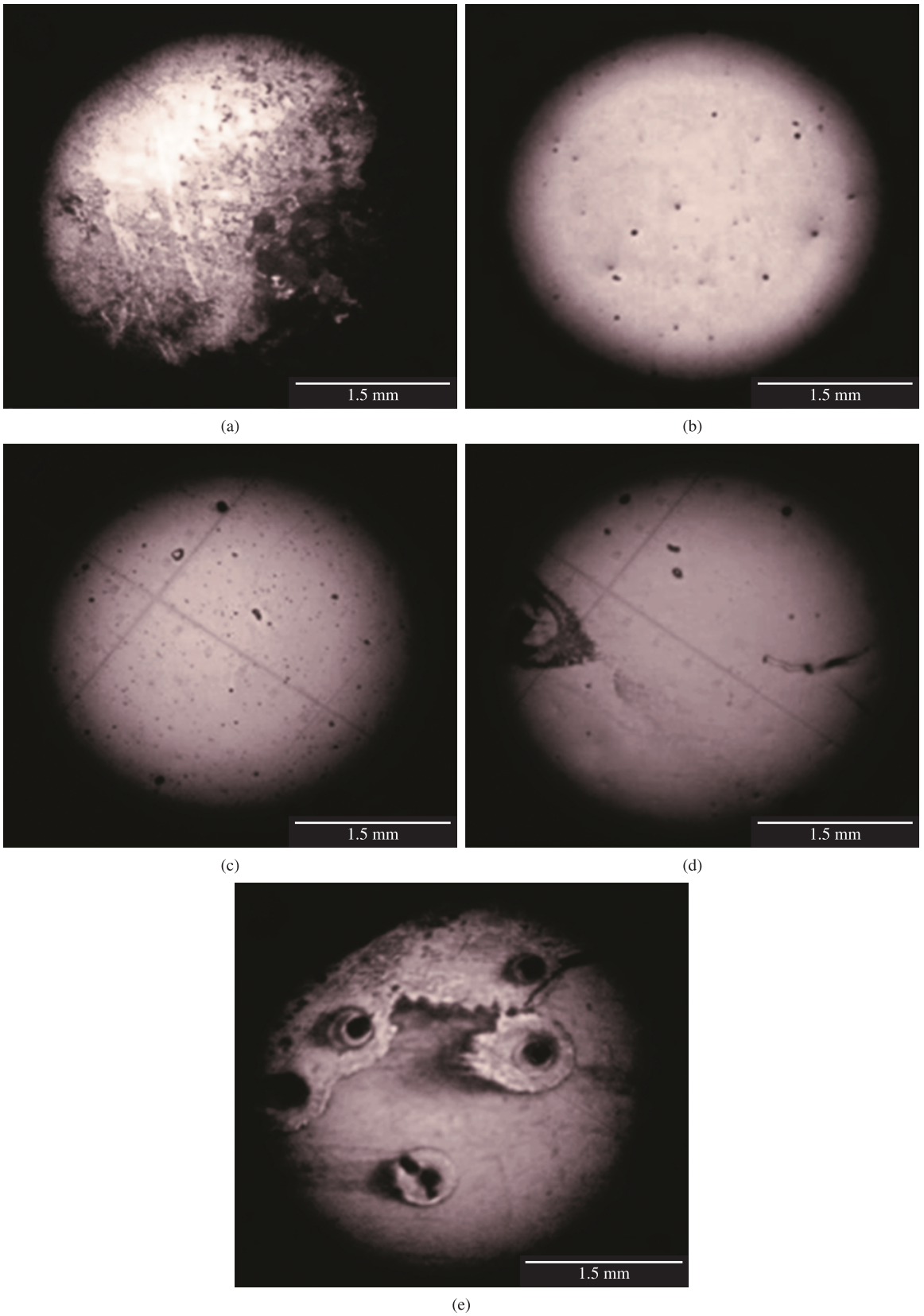

Figure 8. Optical microscopy images of (a) uncoated H13 steel substrate, and deposited H13/Al-Cr-N systems at (b) 40 W, (c) 50 W, (d) 60 W, (e) 70 W.

different powers, where the coating deposited at a power of 40 W has the Al-Cr-N cubic phase, which exhibits the most important effect of corrosion resistance[10], while at other powers, different microstructures were yielded, composed of a mixture of different phases. The film deposited at a power of 70 W offered less resistance to corrosion. In addition, at lower applied powers (40 and 50 W) the presence of Cr and Al oxides could improve the corrosion resistance behavior of the all protective system.

Acknowledgements

This work was financially supported by "El patrimonio Autónomo Fondo Nacional de Financiamiento para la Ciencia, la Tecnología y la Innovación Francisco José de Caldas" under contract RC-No. 275-2011 with CENM, Colombia. The authors thank Dr. Liliana Tirado from the Optoelectronics Laboratory at Universidad del Quindio for her help with X-ray studies.

References

1. Spain E, Avelar-Batista JC, Letch M, Housden J and Lerga B. Characterisation and applications of Cr–Al–N coatings. *Surface and Coatings Technology*. 2005; 200(5-6):1507-1513. http://dx.doi.org/10.1016%2Fj.surfcoat.2005.08.086
2. Caicedo JC, Cabrera G, Caicedo HH, Amaya C and Aperador W. Nature in corrosion-erosion surface for [TiN/TiAlN]n nanometric multilayers growth on AISI 1045 steel. *Thin Solid Films*. 2012; 520:4350-4361. http://dx.doi.org/10.1016%2Fj.tsf.2012.02.061
3. Cabrera G, Caicedo JC, Amaya C, Yate L, Muñoz Saldaña J and Prieto P. Enhancement of mechanical and tribological properties in AISI D3 steel substrates by using a non-isostructural CrN/AlN multilayer coating. *Materials Chemistry and Physics*. 2011; 125:576-586. http://dx.doi.org/10.1016%2Fj.matchemphys.2010.10.014
4. Chen L, Du Y, Wang SQ and Li J. Comparative research on physical and mechanical properties of (Ti, Al)N and (Cr, Al)N PVD coatings with high Al content. *International Journal of Refractory Metals & Hard Materials*. 2007; 25:400-404. http://dx.doi.org/10.1016%2Fj.ijrmhm.2006.11.006
5. Creus J, Billard A and Sanchette F. Corrosion behaviour of amorphous Al–Cr and Al–Cr–(N) coatings deposited by dc magnetron sputtering on mild steel substrate. *Thin Solid Films*. 2004; 446:1-9. http://dx.doi.org/10.1016%2Fj.tsf.2003.11.315
6. Bertrand G, Mahdjoub H and Meunier C. A study of the corrosion behaviour and protective quality of sputtered chromium nitride coatings. *Surface and Coatings Technology*. 2000; 126 (2-3):199-209. http://dx.doi.org/10.1016%2FS0257-8972%2800%2900527-2
7. Reichelt K and Jiang X. The preparation of thin films by physical vapour deposition methods. *Thin Solid Films*. 1990; 191:91-126. http://dx.doi.org/10.1016%2F0040-6090%2890%2990277-K
8. Ding X-Z and Zeng XT. Structural, mechanical and tribological properties of CrAlN coatings deposited by reactive unbalanced magnetron sputtering. *Surface and Coatings Technology*. 2005; 200(5-6):1372-1376. http://dx.doi.org/10.1016%2Fj.surfcoat.2005.08.072
9. Liu C, Bi Q and Matthews A. EIS comparison on corrosion performance of PVD TiN and CrN coated mild steel in 0.5 N NaCl aqueous solution. *Corrosion Science*. 2001; 43(10):1953-1961. http://dx.doi.org/10.1016%2FS0010-938X%2800%2900188-8
10. Lee JH, Ahn SH and Kim JG. Effect of Al additions in WC-($Cr_{1-x}Al_x$)N coatings on the corrosion resistance of coated AISI D2 steel in a deaerated 3.5 wt.% NaCl solution. *Surface and Coatings Technology*. 2005; 190(2-3):417-427. http://dx.doi.org/10.1016%2Fj.surfcoat.2004.03.054
11. Nam KH, Jung YM and Han JG. A comparative study of microstructure and mechanical properties for CrNx films with various deposition rates by magnetron sputtering. *Surface and Coatings Technology*, 2001; 142-144:1012-1016. http://dx.doi.org/10.1016%2FS0257-8972%2801%2901094-5
12. Kawate M, Hashimoto AK and Suzuki T. Oxidation resistance of $Cr_{1-X}Al_XN$ and $Ti_{1-X}Al_XN$ films. *Surface and Coatings Technology*. 2003; 165(2):163-167. http://dx.doi.org/10.1016%2FS0257-8972%2802%2900473-5
13. Ding X-Z, Tan ALK, Zeng XT, Wang C, Yue T and Sun CQ. Corrosion resistance of CrAlN and TiAlN coatings deposited by lateral rotating cathode arc. *Thin Solid Films*. 2008; 516(16):5716-5720. http://dx.doi.org/10.1016%2Fj.tsf.2007.07.069
14. Scheerer H, Hoche H, Broszeit E, Schramm B, Abele E and Berger C. Effects of the chromium to aluminum content on the tribology in dry machining using (Cr,Al)N coated tools. *Surface and Coatings Technology*. 2005; 200:203-207. http://dx.doi.org/10.1016%2Fj.surfcoat.2005.02.112
15. Yang B, Chen L, Chang KK, Pan W, Peng YB, Du Y et al. Thermal and thermo-mechanical properties of Ti–Al–N and Cr–Al–N coatings. *International Journal of Refractory Metals and Hard Materials*. 2012; 35:235-240. http://dx.doi.org/10.1016%2Fj.ijrmhm.2012.06.007
16. Deng J, Wu F, Lian Y, Xing Y and Li S. Erosion wear of CrN, TiN, CrAlN, and TiAlN PVD nitride coatings. *International Journal of Refractory Metals and Hard Materials*. 2012; 35:10-16. http://dx.doi.org/10.1016%2Fj.ijrmhm.2012.03.002
17. Panjan P, Kek Merl D, Zupanič F, Čekada M and Panjan M. SEM study of defects in PVD hard coatings using focused ion beam milling. *Surface and Coatings Technology*. 2008; 202:2302-2305. http://dx.doi.org/10.1016%2Fj.surfcoat.2007.09.033
18. Bobzin K, Bagcivan N, Immich P, Bolz S, Cremer R and Leyendecker T. Mechanical properties and oxidation behaviour of (Al,Cr)N and (Al,Cr,Si)N coatings for cutting tools deposited by HPPMS. *Thin Solid Films*. 2008; 517(3):1251-1256. http://dx.doi.org/10.1016%2Fj.tsf.2008.06.050
19. Wasa K and Huyakawa S. *Handbook of Sputter Deposition Technology*. Noyes Publications; 1992.
20. Lin J, Mishra B, Moore JJ and Sproul WD. Microstructure, mechanical and tribological properties of $Cr_{1-x}Al_xN$ films deposited by pulsed-closed field unbalanced magnetron sputtering (P-CFUBMS). *Surface and Coatings Technology*. 2006; 201(7):4329-4334. http://dx.doi.org/10.1016%2Fj.surfcoat.2006.08.090
21. Li T, Li M and Zhou Y. Phase segregation and its effect on the adhesion of Cr–Al–N coatings on K38G alloy prepared by magnetron sputtering method. *Surface and Coatings Technology*. 2007; 201(18):7692-7698. http://dx.doi.org/10.1016%2Fj.surfcoat.2007.02.044

22. Sugishima A, Kajioka H and Makino Y. Phase transition of pseudobinary Cr–Al–N films deposited by magnetron sputtering method. *Surface and Coatings Technology*. 1997; 97(1-3):590-594. http://dx.doi.org/10.1016%2FS0257-8972%2897%2900402-7

23. Hirai M, Ueno Y, Suzuki T and Jiang W. Characteristics of (Cr_{1-x}, Al_x)N Films Prepared by Pulsed Laser Deposition. *Japanese Journal of Applied Physics*. 2001; 40:1056-1060. http://dx.doi.org/10.1143%2FJJAP.40.1056

24. Banakh O, Schmid PE, Sanjines R and Levy F. High-temperature oxidation resistance of $Cr_{1-x}Al_xN$ thin films deposited by reactive magnetron sputtering. *Surface and Coatings Technology*. 2003; 163-164:57-61. http://dx.doi.org/10.1016%2FS0257-8972%2802%2900589-3

25. Chang Y-Y and Wang D-Y. Corrosion behavior of CrN coatings enhanced by niobium ion implantation. *Surface and Coatings Technology*. 2004; 188-189:478-483. http://dx.doi.org/10.1016%2Fj.surfcoat.2004.08.057

26. Ahn SH, Yoo JH, Choi YS, Kim JG and Han JG. Corrosion behavior of PVD-grown WC–($Ti_{1-x}Al_x$)N films in a 3.5% NaCl solution. *Surface and Coatings Technology*. 2003; 162:212-221. http://dx.doi.org/10.1016%2FS0257-8972%2802%2900519-4

27. Merl DK, Panjan P, Čekada M and Maček M. The corrosion behavior of Cr-(C,N) PVD hard coatings deposited on various substrates. *Electrochimica Acta.* 2004; 49:1527-1533.

28. Da Silva LLG, Ueda M and Nakazato RZ. Enhanced corrosion resistance of AISI H13 steel treated by nitrogen plasma immersion ion implantation. *Surface and Coatings Technology*. 2007; 201(19-20):8291-8294. http://dx.doi.org/10.1016%2Fj.surfcoat.2006.03.063

29. Matthes B, Brozeit E, Aromaa J, Ronkainen H, Hannula SP, Leyland A et al. Corrosion performance of some titanium-based hard coatings. *Surface and Coatings Technology*. 1991; 49(1-3):489-495. http://dx.doi.org/10.1016%2F0257-8972%2891%2990105-6

30. Creus J, Mazille H and Idrissi H. Porosity evaluation of protective coatings onto steel, through electrochemical techniques. *Surface and Coatings Technology*. 2000; 130(2-3):224-232. http://dx.doi.org/10.1016%2FS0257-8972%2899%2900659-3

31. Merl DK, Panjan P, Panjan M and Čekada M. The Role of Surface Defects Density on Corrosion Resistance of PVD Hard Coatings. *Plasma Processes and Polymers*. 2007; 4:S613-S617. http://dx.doi.org/10.1002%2Fppap.200731416

32. Dong H, Sun Y and Bell T. Enhanced corrosion resistance of duplex coatings. *Surface and Coatings Technology*. 1997; 90(1-2):91-101. http://dx.doi.org/10.1016%2FS0257-8972%2896%2903099-X